

Comparison of photon transport efficiency in simple scintillation electron detector configurations for scanning electron microscope

Petr Schauer 

Electron Microscopy Division, Institute of Scientific Instruments of the CAS, Brno, Czech Republic

Correspondence

Petr Schauer, Institute of Scientific Instruments of the CAS, Královopolská 147, CZ-61264 Brno, Czech Republic.
Email: petr@isibrno.cz

Funding information

Czech Academy of Sciences, Grant/Award Numbers: RVO, 68081731; Technology Agency of the Czech Republic, Grant/Award Number: TN01000008

Review Editor: Paul Verkade

Abstract

The purpose of this paper is to find some general rules for the design of robust scintillation electron detectors for a scanning electron microscope (SEM) that possesses an efficient light-guiding (LG) system. The paper offers some general instructions on how to avoid the improper design of highly inefficient LG configurations of the detectors. Attention was paid to the relevant optical properties of the scintillator, light guide, and other components used in the LG part of the scintillation detector. Utilizing the optical properties of the detector components, 3D Monte Carlo (MC) simulations of photon transport efficiency in the simple scintillation detector configurations were performed using the computer application called SCIUNI to assess shapes and dimensions of the LG part of the detector. The results of the simulation of both base-guided signal (BGS) configurations for SE detection and edge-guided signal (EGS) configurations for BSE detection are presented. It is demonstrated that the BGS configuration with a matted disc scintillator exit side connected to the cylindrical light guide without optical cement is almost always a sufficiently efficient system with a mean LG efficiency of about 20%. It is simulated that poorly designed EGS strip configurations have an extremely low mean LG efficiency of only 0.01%, which can significantly reduce detector performance. On the other hand, no simple nonoptimized EGS configuration with a light guide widening to a circular or square profile, with a polished cemented scintillator and with an indispensable hole in it has a mean LG efficiency lower than 6.5%.

KEYWORDS

light guide, MC simulation, scintillator, SEM electron detector

Research Highlights

A perfectly designed light-guiding part of the scintillation detector with high photon transport efficiency is a significant benefit of the imaging system in SEM. The computer-optimized design can improve the geometry and materials of the scintillation detector.

1 | INTRODUCTION

In a scanning electron microscope (SEM), the image is formed by signal electrons generated after the interaction of a primary electron

beam with a specimen surface (Reimer, 2013c). The image quality of an SEM is largely determined by the performance of an electron detector. Scintillation electron detectors (Everhart & Thornley, 2004) are mainly used in SEMs to detect signal electrons. A priority feature

of a high-quality scintillation electron detector is its strong modulation transfer function (MTF). The MTF is a variant of the optical transfer function (OTF) that neglects phase effects, but it is equivalent to the OTF in many situations. Only the use of an extremely fast scintillator with a short decay time and a low afterglow guarantees a strong MTF of the entire imaging system (Goodman, 2005; Williams, 1998; Williams & Becklund, 2002). Much attention is necessarily paid to the MTF of the scintillation electron detector in the SEM (Bok & Schauer, 2014b; Saiga et al., 2018; Schauer et al., 2019). However, attention must also be paid to the detective quantum efficiency (DQE) of the scintillation electron detector, which is based on the signal-to-noise ratio (Comins & Thirlwall, 1981; Joy et al., 1996; Oatley, 1985; Reimer, 2013b). The low efficiency of the detector reduces DQE and thus the performance of the entire SEM imaging system.

Unfortunately, the efficiency of the scintillation electron detector is often simplified and is referred to as the electron-photon energy conversion efficiency in scintillator cathodoluminescence (CL) centers, and the utilization of generated signal photons is abandoned (Everhart & Thornley, 2004; Frank, 2002; Healy & Mott, 2016; Nedela et al., 2018). However, the process of photon collection can be greatly inefficient. If the scintillator possesses high optical self-absorption, its conductive coating has low optical reflectance, it is incorrectly coupled to the light guide, and/or the light guide is incorrectly designed, the photon collection efficiency at the PMT photocathode of the scintillation electron detector can only be in the order of units of percent or less. These problems need attention. Estimation and experimental verification of the photon transfer efficiency of the scintillation detection system are too time-consuming and expensive and offer uncertain results. Therefore, in this paper, attention will be paid to the relevant optical properties of the scintillator, light guide, optical cement, and other components used in the scintillation electron detector for SEM. Simulations of photon transport efficiency in the simple scintillation electron detector configurations for SEM will be performed and presented in this paper utilizing optical characterization of the detector components.

The simulation of photon transport efficiency in the scintillation electron detector for SEM has only rarely been published. Such a simulation can be based on a quantitative analytical or MC approach. Both of these approaches can be implemented in either a simplified 2-dimensional (2D) or a full 3-dimensional (3D) layout. Unfortunately, some publications offer only a 2D analysis of the photon collection, simplifying the problem only to a rough estimate (Danilatos, 2012). If a quantitative analytical approach is chosen, only simple system geometries with a high symmetry can be calculated (Carrier & Lecomte, 1990b; Filippov et al., 2001). A method that makes use of an MC simulation is more generally applicable. It does not depend on the simulated systems' symmetry, but some works are still limited to parallelepipeds (Carrier & Lecomte, 1990a; Lerche et al., 2008; Xiaoguang, 1984) and others to rotational symmetries (Schauer & Autrata, 1992). The universal 3D MC method, intended for nearly any scintillation detection system for S(T)EM, is the SCIUNI application (Schauer, 2007). The MC simulations of light collection from the

scintillators are more commonly used to design the detectors in the field of high-energy physics, especially in medical scintillography techniques. There are various commercial or freely available programs such as ZEMAX (Bauer et al., 2009; Lorincz et al., 2010; Salomoni et al., 2018) or GEANT (Badiei et al., 2019; Knyazev et al., 2021; van der Laan et al., 2010). However, the common disadvantage of these programs is that they are not suitable for an overly complex geometry of the scintillator or light guide, which cannot be avoided in the SEM detectors.

Two different basic image modes are used in the SEM (Reimer, 2013d). These are (1) the secondary electron image mode (SE mode), where the detector is located outside the primary electron beam, and (2) the complementary backscattered electron image mode (BSE mode), where the detector must be located above the specimen in the primary electron beam path of the SEM (Reimer, 2013a; Zhou et al., 2006). The SE mode makes use of the standard Everhart-Thornley detector (Everhart & Thornley, 2004), that is, a base-guided signal (BGS) rotationally symmetric scintillation detection system. The BSE mode requires the use of a Robinson-type flat plate scintillator with a hole for the primary electron beam and thus allows the light signal to be collected only from the side edge of the scintillator (Robinson, 1980). Therefore, the BSE mode must use an edge-guided signal (EGS) system that has a much lower symmetry than the BGS one and is thus much less suitable for efficient light collection from the scintillator. Furthermore, the EGS detector design must comply with the space available in the microscope chamber. All these facts can result in complicated EGS detector geometry.

To simulate the photon transport efficiency in the scintillation electron detector for SEM, it is necessary to obtain and use not only a suitable computer application for the simulation, but also to know or experimentally determine the input simulation parameters. The simulation parameters, in this case, are the CL emission spectrum of the scintillator and the optical properties, shapes, and dimensions of all components (objects) of the entire scintillation detector configuration. Appropriate methods must be used to prepare the samples of the components and to determine their spectral properties. The components must be examined by suitable methods and later entered into the simulation. The following components are considered here: (1) the scintillator and (2) its anticharging coating, (3) the light guide, and (4) the optical cement. Only on the basis of high-quality optical characterization of these detector components it is possible to proceed with the implementation of the photon transport efficiency simulation in the scintillation electron detector. A sufficiently useful value of such a simulation can only be guaranteed when using a high-quality 3D MC model.

In our previous papers, some topics have been focused on the computer-optimized design (COD) of the light-guiding (LG) parts of the scintillation electron detectors for SEM (Schauer, 2007; Schauer & Autrata, 2000; Schauer et al., 2021). However, these previous studies usually do not allow comparing the influence of individual parameters of the LG systems, such as the configuration, shape, or size. The purpose of this paper is not to determine the efficiencies of specific complex scintillation electron detectors for specific microscopes, but to

find some general rules for the design of the robust scintillation electron detectors for an SEM that possesses an efficient LG system. Such design rules can give at least some general guidance on how to avoid the improper design of extremely inefficient configurations of the scintillation electron detectors. These general design rules would be the basis for choosing a shape and material, but it is not possible to get the best efficiency without subsequent optimization.

2 | MATERIALS AND METHODS

2.1 | Simulated materials

The YAG:Ce single crystal (Ce^{3+} activated yttrium aluminum garnet- $\text{Y}_3\text{Al}_5\text{O}_{12}:\text{Ce}^{3+}$) was chosen as the scintillator for the simulation. The YAG:Ce scintillator, grown with the Czochralski method in Crytur Ltd. and finished as described in our previous papers (Schauer et al., 2019; 2021), was used for experimental determination of its CL emission spectra and its optical properties. The dimensions of the scintillator for the simulation are given in Table 1 together with the dimensions of the other simulated materials. The size of the hole in the scintillator, which is indispensable for the passage of the primary electron beam in the EGS scintillation systems for BSE detection, is also tabulated.

A thin film of Al in the rotationally symmetric BGS configurations for SE detection and a thin film of indium tin oxide (ITO) in the EGS configurations for BSE detection were chosen as anticharging coatings of the scintillators for the simulation. To experimentally determine the optical properties of both coatings, the films were deposited onto quartz substrates using a radiofrequency (RF) sputtering unit with 152 mm cathodes in the RF mode as schematically drawn in our previous paper (Schauer et al., 2021). Reactive sputtering was performed in argon and argon-oxygen atmospheres, respectively. The

argon and oxygen fluxes were regulated with high-accuracy by mass-flow controllers. Norland Optical Adhesive NOA 61 optical cement was chosen as a scintillator-light guide interface binder. The optical properties of the cement were taken from the manufacturer (Norland, 2021). The thicknesses of the films and cement are also given in Table 1. Optical polymethyl methacrylate (PMMA) was chosen as a light guide for the simulation. Although commercial PERSPEX, commercial Merci silicate glass, and quartz are also suitable materials, PMMA has been selected for its suitable optical properties, being the cheapest and easiest to machine.

2.2 | Material characterization methods

The CL spectrum of the scintillator was measured using the equipment built in our laboratory (Bok & Schauer, 2014a). The method is described in more detail in our earlier paper (Schauer et al., 2019). The CL spectrum was measured using an e-beam energy of 10 keV and an excitation current of 30 nA, a spot diameter of 2 mm, and a wavelength range of 450 nm to 750 nm at room temperature. Although the apparatus allows measurements in a much broader spectral region, in this case, attention was focused only on the region of the characteristic emission band of YAG:Ce. The Hamamatsu R943-02 PMT was used for spectra detection. The CL spectrum was corrected for the spectral response of the apparatus.

The optical properties of the YAG:Ce single crystal scintillator and the PMMA light guide were obtained using the double-beam UV-VIS-NIR spectrophotometer Varian Cary 5. Measurements were made both in the reference sample mode and nonreference sample mode. In the case of the reference sample measurements, a suitable reference sample of different thickness was used for the optical transmittance measurement. When measured without the reference

TABLE 1 The dimensions of the simulated scintillators, light guides, optical cement, and coatings. The size of the hole in the scintillator is also tabulated

Object	Dimensions (mm)				
	Diameter ^a (mm)	Side ^b (mm)	Height ^c (mm)	Length ^d (mm)	Thickness ^e (mm)
Disc scintillator	20	n/a	2	n/a	n/a
Cone scintillator	20	n/a	5	n/a	n/a
Hemispherical scintillator	20	n/a	10	n/a	n/a
Hole in scintillator	2	n/a	2	n/a	n/a
PMMA light guide	20	20	n/a	60	n/a
Optical cement NOA 61	area ^f	area ^f	n/a	n/a	1E-2 to 22E-2
ITO coating ^g	20	n/a	n/a	n/a	5.0E-6
Al coating ^g	20	n/a	n/a	n/a	5.0E-5

^aDiameters are applicable only for the rotationally symmetric objects.

^bSides are applicable only for the parallelepiped objects.

^cHeights are applicable only for the scintillators and holes.

^dLengths are applicable only for the light guides.

^eThicknesses are applicable only for the optical cements and coatings.

^fAreas of the optical cement are determined by the exit surfaces of the scintillators.

^gCoatings are determined by the electron excited surfaces of the scintillators.

sample, the obtained values were corrected for reflectivity using the refractive index. The optical transmittances of the YAG:Ce scintillator and PMMA light guide were measured on 10 mm and 50 mm long cylindrical samples, respectively, using a wavelength range of 450–750 nm. Although the spectrophotometer allows measurements in a much broader spectral region, in this case, attention was focused only on the region of the characteristic emission band of YAG:Ce.

The refractive indices for all samples were obtained with the minimum deviation method (Kuwano et al., 1988). The optical reflectivity at the internal scintillator-coating boundary was calculated using the matrix method (Knittel, 1976). The optical reflectivity was measured using the spectroscopic reflectometry method to verify these calculated results experimentally (Ohlídal & Navrátil, 1984).

2.3 | Photon transport simulation method

The MC simulation of the photon transport from scintillator luminescence centers to a photomultiplier (PMT) photocathode was used to determine the efficiency of light signal collection from the scintillator (Schauer, 2007). The application used is called SCIUNI, and it is primarily intended for the COD of the scintillation electron detectors for SEMs. The method uses photon generation from a luminescent center in a random direction and monitors the 3D photon trajectory and the probability that the photon will reach the photocathode. By repeating this process about 10 thousand times, the method can calculate the efficiency of the LG configuration of the electron detector for SEM.

The model includes mirror reflection by a metal-coated surface, Fresnel reflection by a metal-uncoated surface, Fresnel passage through the boundary of different materials, diffusion reflection, and passage through a matted surface, and optical absorption in material. The method allows simulating photon transport in nearly arbitrary scintillator and/or light guide shapes. The SCIUNI application can run on UNIX and Windows operating systems. The simulation results presented in this paper were obtained using the FreeBSD UNIX operating system. The result of the simulation is the signal transfer efficiency of the SEM scintillation detector.

The method enables the comparison of the signal transfer efficiencies of the different scintillation detectors with specific scintillator or light guide optical properties and can optimize the shapes and sizes of both scintillators and light guides. Optimization can be achieved using a dimension-stepping algorithm of changes of the individual geometric values, but this was not used in the simulation of the nonoptimized simple light guides in this paper. Using SCIUNI, the signal transfer efficiencies can be obtained either as mean, minimum, or maximum values independent of the signal electron impact location or in the form of 3D surface or contour graphs depending on the impact location. In this paper, attention will be focused only on the mean, minimum, and maximum values of the photon transport efficiencies of the relatively simple scintillation electron detector configurations.

3 | RESULTS

Simulation results of photon transport efficiency in scintillation electron detector configurations for SEM cannot be obtained without the knowledge of simulation parameters. In addition to the shapes and dimensions of all objects of the entire configuration of the scintillation detector, it is necessary to know the optical properties of these objects. In the case of the scintillator, we must also know its CL emission spectrum. Thus, the results of the characterization of the materials included in the simulation will be presented first.

3.1 | Simulated material characterization

The results concerning the YAG:Ce scintillator as well as all other materials, such as the anticharging (conductive) coating, light guide, and optical cement, will be presented in this section.

CL efficiency, CL emission spectrum, and especially CL kinetics are crucial properties for assessing the performance of a scintillator in an electron detector for SEM. However, only the CL emission spectrum is important for assessing the LG properties of the scintillator. The CL spectrum measurement of the YAG:Ce single crystal scintillator was performed using the experimental equipment described in Section 2.2. The CL spectrum measurement cannot be performed without some anticharging coating. Therefore, using the RF sputtering method described in Section 2.1., 50 nm of Al was applied to the scintillator surface, which was excited by an electron beam during the CL spectrum measurement. No corrections were made to the effect of the coating. Unless otherwise noted, the scintillator here means not only the single crystal itself but also the conductive coating on its surface. The CL emission spectrum of the YAG:Ce single crystal scintillator is shown in Figure 1. The CL intensity (left axis of the graph) is normalized to the maximum of the CL emission, so it is expressed in

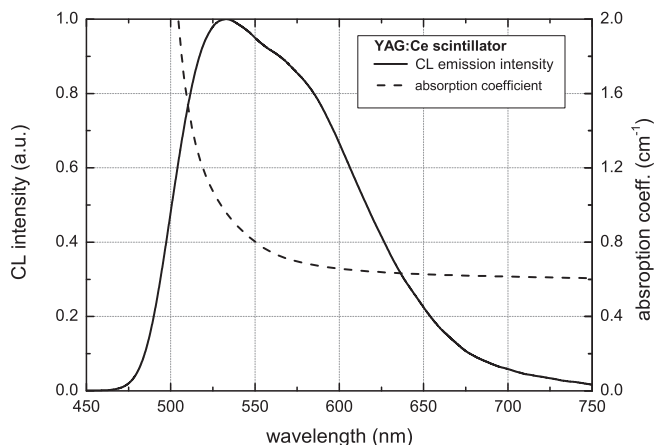


FIGURE 1 The CL emission spectrum (left axis) and the spectrum of the optical absorption coefficient (right axis) of the YAG:Ce single crystal scintillator. The emitted CL intensity is normalized to the maximum of the CL emission, so it is expressed in relative (arbitrary) units

relative (arbitrary) units. The spectrum was measured only in the wavelength range of the characteristic emission band of YAG:Ce (from 450 nm to 750 nm) at room temperature. The results were corrected for the device's spectral transmittance and detector spectral sensitivity. It can be read from the graph that the maximum emission of YAG:Ce lies at 533 nm and the full width at half maximum (FWHM) lies in the range from 501 nm to 617 nm so that the center of the emission band corresponds to the wavelength of 559 nm. This wavelength of the emission band center is decisive for assigning optical parameters for the simulation.

A necessary condition for a robust scintillation detection system in SEM is to collect a light signal from the scintillator with a minimum of losses. High optical self-absorption and/or a high refraction index of the YAG:Ce scintillator can significantly reduce the performance of the entire detector. The spectral dependence of the optical transmittance of the 10 mm long YAG:Ce scintillator was measured in the spectral range of 450 nm to 750 nm using the double-beam spectrophotometer, as described in Section 2.2. Based on this measurement, the spectral dependence of the optical absorption coefficient of YAG:Ce was calculated. This spectrum is shown in Figure 1 using the right axis of the graph. It is evident that the YAG:Ce scintillator exhibits relatively low optical absorption in the spectral range of its characteristic emission. The absorption coefficient of YAG:Ce and other individual detector components at the wavelength of the YAG:Ce emission band center are tabulated in Table 2. Note that the absorption coefficients in Table 2 are unusually given in mm^{-1} , as the SCIUNI simulation application that will use these parameters requires dimensional inputs in mm.

The spectral dependence of the optical absorption coefficient of the PMMA light guide is shown in Figure 2. This graph (left axis) for the spectral range 450 nm to 750 nm was obtained on the 50 mm long sample using the same measurement as for the YAG:Ce scintillator. The absorption coefficient of this high-quality optical PMMA is two orders of magnitude lower than the YAG:Ce scintillator. The absorption coefficient of the NOA 61 optical cement is also plotted and tabulated in Figure 2 and Table 2, respectively. The magnitude of the absorption coefficient of the cement is much less important than the magnitude of the absorption coefficients of the scintillator and the light guide since the cement is applied at a thickness of only 10 μm to 20 μm in the scintillation system, as shown in Table 1.

Using the optical transmittance measurements in the reference sample mode described in Section 2.2, the refractive indices of both YAG:Ce single crystal scintillator and LG components were determined. The results of the dependence of the refractive indices on the wavelength for YAG:Ce, PMMA, and ITO are shown in Figure 2 (right axis of the graph). The refractive indexes of the individual detector components at the wavelength of the YAG:Ce emission band center are tabulated in Table 2. The accuracy of the refractive index of the optical cement is not important, since any value between the refractive indices of the light guide and the scintillator guarantees the same transmission efficiency of the signal photons from the scintillator to the light guide. However, the refractive index of the scintillator that is much higher than the refractive index of the light guide can significantly prevent the efficient collection of the signal photons in the scintillation detector in SEM. The value of the refractive index of YAG:Ce is not ideal. It would be more advantageous to have the refractive index value of YAG:Ce equal to or only slightly higher than the refractive index value of the light guide.

To better imagine the influence of the refractive indices on the internal optical reflectivity or transmissivity of different optical boundaries in the detection system, the results of the refractive indices were

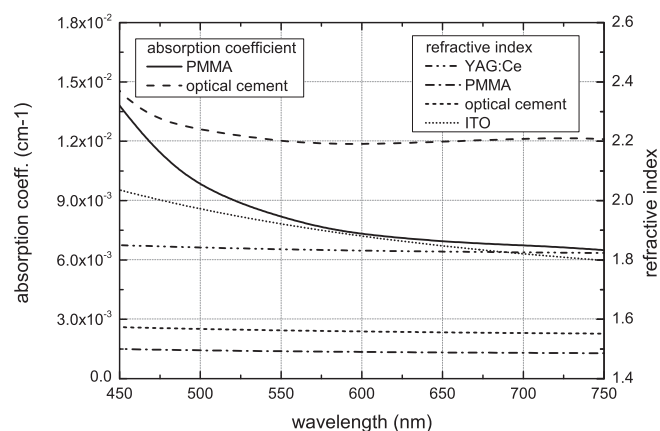


FIGURE 2 The spectral dependence of the optical absorption coefficients (left axis) and the refractive indices (right axis) of the LG materials applied in the simulation. See Figure 1 for the absorption coefficient of the YAG:Ce single crystal

TABLE 2 Optical parameters applied in the simulation

Object	Absorption coef. ^a (mm^{-1})	Refraction index ^a	Optical reflectivity (%)	Critical angle ^b to vacuum (deg)	Critical angle to PMMA (deg)	Critical angle to cement (deg)
YAG:Ce scintillator	0.0743	1.84	100 ^c	32.9	54.1	58.0
PMMA light guide	0.000816	1.49	100 ^c	42.2	n/a	n/a
Optical cement NOA 61	0.0012	1.56	100 ^c	39.9	72.8	n/a
ITO coating	n/a	1.92	100 ^c	31.4	50.9	54.3
Al coating	n/a	n/a	80 ^a	n/a	n/a	n/a

^aFor a wavelength of 559 nm (the center of the YAG:Ce emission band).

^bThe smallest angle of incidence that yields total internal reflection to the given boundary.

^cOnly for total internal reflection.

used to calculate the dependence of the optical reflectivity on the light incidence angle to these boundaries. The angle of incidence here means the deviation from the perpendicular to the boundary surface. The dependences of the internal optical reflectivity on the incidence angle for the YAG:Ce-vacuum, PMMA-vacuum, YAG:Ce-cement, ITO-vacuum, ITO-YAG:Ce, cement-PMMA, and YAG:Ce-PMMA interfaces are shown in Figure 3. The dependences were calculated using the Fresnel equations (Born & Wolf, 1999), assuming mirror reflection and equality of parallel and perpendicular polarization. It is important to know that the optical transmissivity of the listed boundaries is the remaining portion of the light that is not reflected. The critical angle is the smallest angle of incidence that yields total reflection. The critical angles for the individual boundaries are noticeable in Figure 3. The values of the critical angles that are significant in the simulation of photon transport efficiency in the scintillation detector are given in Table 2.

All the results of the optical characterization of the detector components presented in this section (numerically shown in Table 2) together with data of the shapes and dimensions of both scintillator and light guide (given in Table 1) are needed for the MC simulations of photon transport efficiency in the simple scintillation electron detector configurations for SEM. Using these parameters the results of the SCIUNI MC simulation will be presented in the following Section 3.2.

3.2 | Simulation results

The results of the photon transport efficiency simulation of both BGS configurations for SE detection and edge-guided signal (EGS) configurations for BSE detection are presented in this section. As already mentioned, the EGS detection system must be located above the specimen in the primary electron beam path of the SEM and must

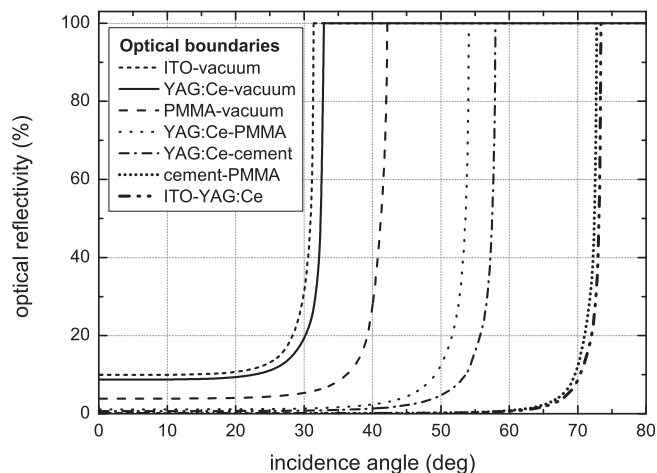


FIGURE 3 The dependence of internal optical reflectivity on the incidence angle for the individual boundaries of the LG system of the scintillation electron detector. The critical angles are recognizable in the graph as the smallest incidence angles that yield total reflection

comply with the space available in the microscope chamber, which can result in complicated geometry. Therefore, it has a much lower symmetry and is thus much less suitable for efficient light collection from the scintillator. In contrast, the BGS configuration makes use of the rotationally symmetric scintillation detection system.

The 3D MC simulation results of the signal photons transport from the luminescence centers for nine simple scintillator - light guide configurations will be presented. The reason is not to determine the efficiencies of specific complex scintillation detectors for specific microscopes, but to find some general rules for the design of robust scintillation electron detectors for an SEM that possesses an efficient LG system. The dependence of photon transport efficiency on the electron impact location, that is, on the location of the luminescent center, will not be reported here to determine the general rules. The results of the simulations of the simplified configurations presented here, which were performed using the SCIUNI application mentioned in Section 2.3 and described in more detail in the previous paper (Schauer, 2007), are only the mean, minimum, and maximum photon transport efficiency from the randomly generated locations on the electron excited scintillator surface.

The results from the previous Section 3.1 were used for the simulation, especially those listed in Table 2 together with data of the shapes and dimensions in Table 1 in Section 2.1. For each configuration, 10,000 randomly generated directions were simulated at each of 1000 randomly generated locations on the scintillator surface.

3.2.1 | Simulation of BGS configurations

The simulation of the efficiencies of photon transport from luminescence centers to the PMT photocathode in the BGS configurations for the SE detectors for SEM is less important than the simulation of the efficiencies in the EGS configurations for BSE detection. The main reason is that the BGS configurations are formed by a rotationally symmetric system with much simpler signal photon guiding. In other words, the BGS configuration has a much higher symmetry than the EGS one and is thus much more appropriate for efficient light collection from the scintillator. Therefore, the BGS configuration gives a much greater chance of obtaining a rough estimate of photon transport efficiency.

Three BGS scintillation detection systems were selected to simulate their photon transport efficiencies. All simulated BGS configurations have the same PMMA cylindrical light guide but differ in scintillator shape, as shown in Figure 4. The (a) configuration UD_V_001 includes the disk plate scintillator, the (b) configuration UK_V_001 includes the conical scintillator, and the (c) configuration UP_V_001 includes the hemispherical scintillator. All dimensions are given in Table 1 in Section 2.1.

The results of photon transport efficiency simulations of the BGS configurations described in Figure 4 are shown in Table 3. Use the configuration ID to link the systems in Figure 4 with those in Table 3. In addition to the efficiency and geometry of the simulated

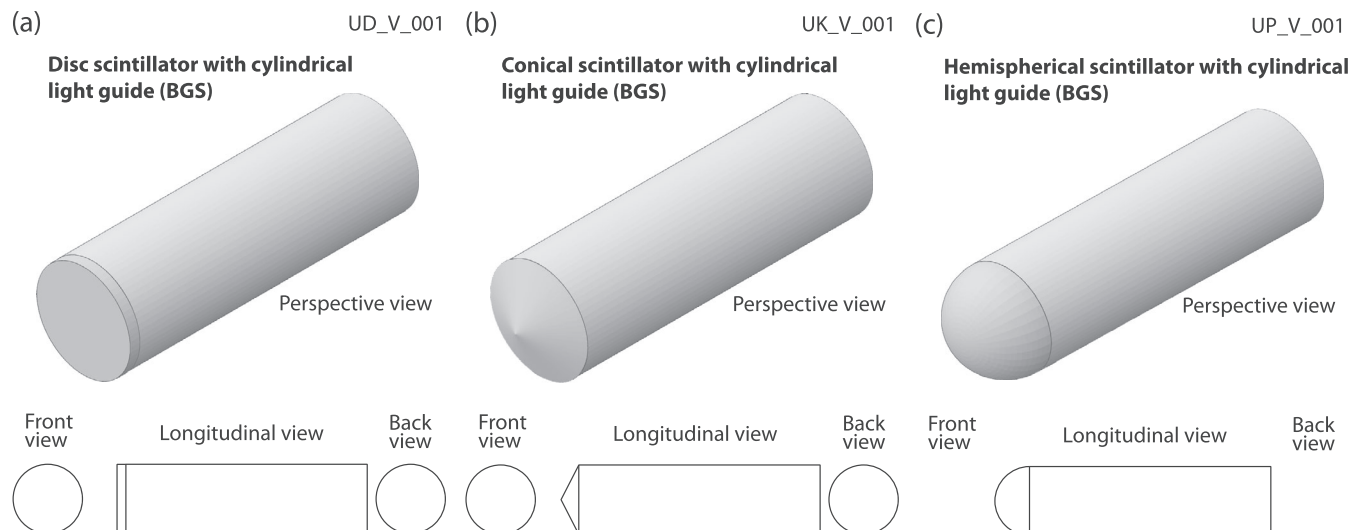


FIGURE 4 The shapes of the simulated BGS scintillation detector configurations with the YAG:Ce single crystal scintillators and the PMMA light guides. See Table 1 for dimensions

TABLE 3 Photon transport efficiency in the different BGS rotationally symmetric systems. The BGS configurations need no hole

Configuration ID	Description	Matted scintillator exit side	Optical cement	Efficiency of photon transport (%)		
				Mean	Min.	Max.
UD_V_001	Disc scintillator with cylindrical light guide	yes	no	18.6	17.4	19.6
		yes	yes	2.5	1.1	3.5
UK_V_001	Conical scintillator with cylindrical light guide	yes	yes	13.8	9.1	15.5
		no	yes	17.9	12.6	35.2
UP_V_001	Hemispherical scintillator with cylindrical light guide	yes	yes	5.07	4.06	8.38
		no	yes	6.8	0.82	13.05

configurations, the machining of the scintillator exit surface and the use of optical cement are also distinguished. Unlike the EGS configurations, optical cement is not indispensable for the BGS configurations due to different scintillator mounting. The BGS configurations require a conductive ring (optically nearly neutral) to provide an accelerating voltage on the scintillator surface. This ring can also mount the scintillator to the light guide. Not only the mean photon transport efficiencies are tabulated, but also the minimum and maximum ones. The difference between the minimum and maximum efficiency indicates the efficiency homogeneity over the electron excited scintillator surface. It is evident from the results that the BGS configuration with a matted disc scintillator exit side connected to the cylindrical light guide without optical cement is not only the most efficient, but also shows the greatest homogeneity of efficiency over the electron excited scintillator surface. In contrast, the often-used configuration with the disc scintillator exit side cemented to the light guide is seven times less efficient and shows lower homogeneity.

The BGS configuration with the conical scintillator connected to the cylindrical light guide is also relatively efficient, but only if a fully polished scintillator cemented to the light guide is used. However, the

efficiency homogeneity of such a configuration is much lower compared to that with the disc scintillator. An increase in efficiency homogeneity of the configuration with the conical scintillator can be ensured by matting the exit side of the scintillator, which is cemented to the light guide, but at the expense of reduced mean photon transport efficiency. The BGS configurations with conical and hemispherical scintillators that are not cemented to the light guide have not been simulated, as it is practically impossible to design these systems with an unfixed scintillator.

The BGS configurations with the hemispherical scintillator connected to the cylindrical light guide are the least efficient. Their mean photon transport efficiency is approximately three times lower than that of configurations with the disc or conical scintillator. The efficiency homogeneity of these configurations with the hemispherical scintillator is approximately the same as that of the configurations with the conical scintillator. The hemispherical scintillator configurations cannot be preferred even in this respect. In addition, the hemispherical scintillators are the most difficult to manufacture, the BGS configurations with the hemispherical scintillator connected to the cylindrical light guide are considered the worst choice of all the BGS configurations simulated in this paper.

3.2.2 | Simulation of EGS configurations

The simulation of the efficiency of the photon transport from luminescence centers to the PMT photocathode in the EGS configurations is indispensable. It is practically impossible to determine the optimal choice of the material, shape, and size of both scintillators and light guides for the particular EGS detector system without a computer application. Improperly designed EGS detection systems can possess poor light guiding efficiency, sometimes below 1%, while computer-optimized ones can achieve efficiencies of up to tens of percent. For the EGS configurations, the scintillators must always be connected to the light guides using optical cement, as no other mounting is applicable.

Six EGS scintillation detection systems were selected to stimulate their efficiency. In fact, two sets of the EGS configurations were simulated. The first set contained three EGS configurations with the same disc (circular plate) YAG:Ce single crystal scintillator but with three different shapes of the PMMA light guides. The only difference between the first and the second set is the shape of the scintillator. All three EGS configurations of the second set have the square plate scintillator, while the shapes of the PMMA light guides are almost the same as those of the first set. All dimensions of the EGS configurations are given in Table 1 in Section 2.1.

The shapes of the first set of the simulated EGS configurations with the circular plate YAG:Ce scintillator are shown in Figure 5. The (a) configuration UDDH_001 includes the strip PMMA light guide, the (b) configuration UDDHR001 includes the PMMA light guide widening to the square profile, and the (c) configuration UDDVR001 includes the PMMA light guide widening to the circular profile. For a better presentation of these EGS configurations, Figure 5 contains not only perspective views but also drawings with the longitudinal

(top and side), front and back views. The scintillators are mounted to the light guides using optical cement.

Results of the photon transport efficiency simulations of the first set of the EGS configurations described in Figure 5 are shown in Table 4. As with the BGS configurations, the configuration ID, system geometry, machining of the scintillator exit surface, as well as the mean, minimum and maximum photon transport efficiency, are tabulated for each EGS configuration. Use of the optical cement is not tabulated, as the scintillators must always be mounted to the light guides with cement in the EGS configurations, as different mounting is impossible. It should be emphasized that all EGS systems must have a hole for primary electron beam passage. However, to assess the effect of the hole on the efficiency of the system, the EGS systems without a hole were also simulated for comparison. The existence or nonexistence of the hole is also indicated in Table 4. For each EGS configuration, four simulations were performed for different scintillator matting and cementing combinations to assess the effect of the modifications.

It is evident from the results that these simple EGS configurations are less efficient than the BGS ones. Systems with the strip light guides appear to have by far the lowest efficiency of this set with the circular plate scintillator. The worst of these strip configurations is that with the polished scintillator exit surface that does not have a hole. This configuration has a mean efficiency of only 0.46%. At the same time, all extremely inefficient strip configurations also have the greatest efficiency inhomogeneity over the electron excited scintillator surface. With these least efficient systems, the ratio of the maximum to minimum efficiency at different locations of the excited scintillator surface sometimes reaches a value of several hundred. On the contrary, the most efficient of this set are both configurations with the widening light guide using the scintillator with the polished exit surface, which achieve an efficiency of nearly 7%. Moreover, they

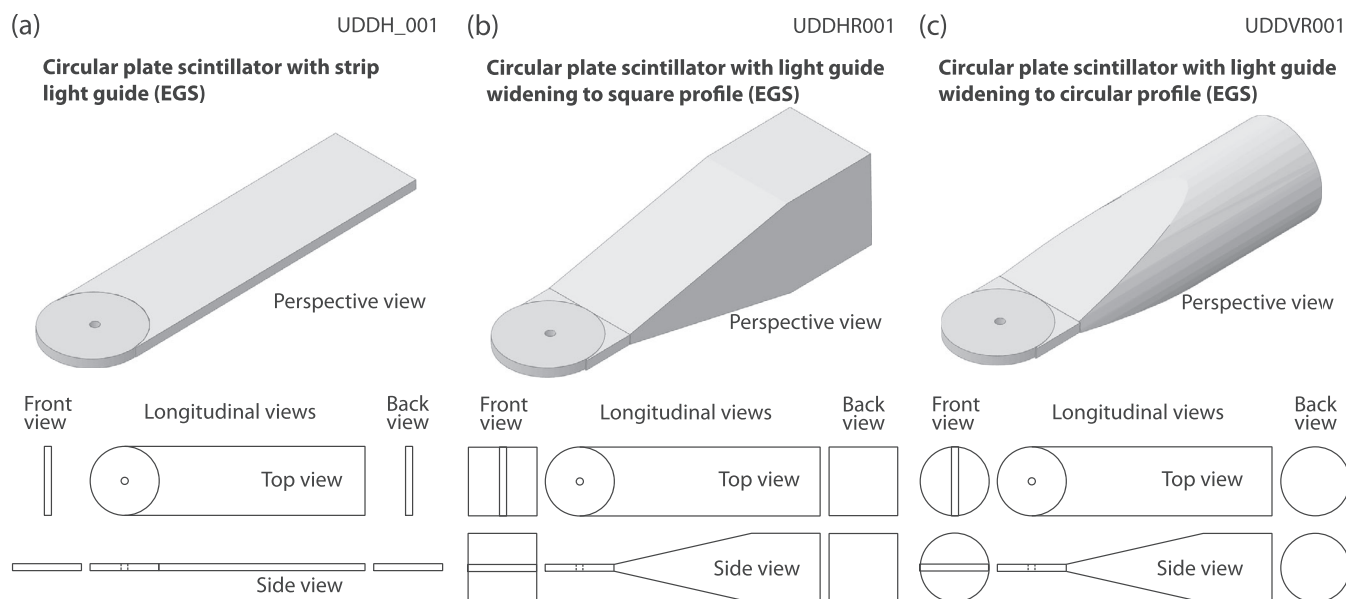


FIGURE 5 The shapes of the simulated EGS scintillation detector configurations with the YAG:Ce circular plate single crystal scintillators and the PMMA light guides. See Table 1 for dimensions

TABLE 4 Photon transport efficiency in the different EGS systems with the circular plate scintillator. The scintillators are mounted to the light guides using optical cement

Configuration ID	Description	Hole in scintillator	Matted scintillator exit side	Efficiency of photon transport (%)		
				Mean	Min.	Max.
UDDH_001	Circular plate scintillator with strip light guide	No	Yes	0.52	0.012	3.16
		Yes	Yes	0.65	0.083	3.18
		No	No	0.46	0.020	3.41
		Yes	No	0.66	0.057	3.41
UDDHR001	Circular plate scintillator with light guide widening to square profile	No	Yes	5.26	1.87	16.29
		Yes	Yes	5.31	1.56	16.38
		No	No	6.98	0.83	18.1
		Yes	No	6.96	0.86	18.14
UDDVR001	Circular plate scintillator with light guide widening to circular profile	No	Yes	5.21	2.04	14.4
		Yes	Yes	5.26	1.44	16.06
		No	No	6.88	1.05	17.4
		Yes	No	6.85	1.02	17.45

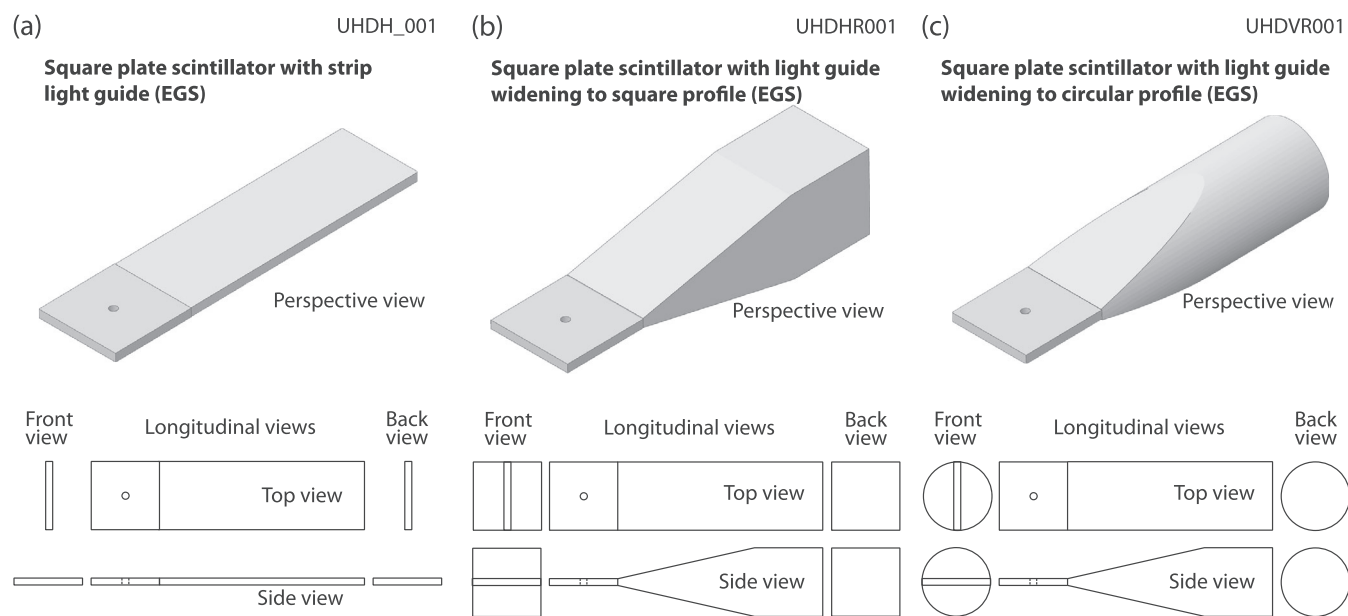


FIGURE 6 The shapes of the simulated EGS scintillation detector configurations with the YAG:Ce square plate single crystal scintillators and the PMMA light guides. See Table 1 for dimensions

show greater efficiency homogeneity over the electron excited scintillator surface, although the ratio of maximum to minimum efficiency at different locations of the excited scintillator surface is around a quite high value of 20.

These results show that the simple EGS configurations are not efficient and satisfactory in terms of collection homogeneity. Although the configuration with the light guide widening to the circular profile is slightly less efficient than that with the light guide widening to the square profile (difference of only 1%), the first configuration is more advantageous because it is easier for the machine. It should be noted that many EGS configurations with a hole are more efficient

than those without a hole. This might be considered surprising. However, with inefficient configurations, the existence of any objects that disrupt the unfavorable geometry of the system can be advantageous. The existence of matting does not have much effect on the EGS system efficiency, as the application of optical cement, which cannot be avoided, largely eliminates matting.

The shapes of the second set of the simulated EGS configurations with the square plate YAG:Ce scintillator are shown in Figure 6. Both sets of the EGS configurations differ only in the different shapes of the scintillator plate. As in the previous figure, the (a) configuration UDDH_001 includes the strip PMMA light guide, the (b) configuration

TABLE 5 Photon transport efficiency in the different EGS systems with the square plate scintillator. The scintillators are mounted to the light guides using optical cement

Configuration ID	Description	Hole in scintillator	Matted scintillator exit side	Efficiency of photon transport (%)		
				Mean	Min.	Max.
UHDH_001	Square plate scintillator with strip light guide	No	Yes	0.066	0.0045	0.34
		Yes	Yes	0.17	0.017	0.89
		No	No	0.012	0.00097	0.17
		Yes	No	0.14	0.011	0.7
UHDHR001	Square plate scintillator with light guide widening to square profile	No	Yes	5.61	1.19	16.74
		Yes	Yes	5.62	1.01	17.02
		No	No	6.49	1.45	17.96
		Yes	No	6.57	0.84	18.5
UHDVR001	Square plate scintillator with light guide widening to circular profile	No	Yes	5.56	1.22	16.04
		Yes	Yes	5.64	1.03	16.81
		No	No	6.44	1.4	20.21
		Yes	No	6.51	0.81	20.73
		No	Yes	2.5	1.1	3.5

UHDHR001 includes the PMMA light guide widening to the square profile, and the (c) configuration UHDVR001 includes the PMMA light guide widening to the circular profile. The drawings of the EGS configurations presented here also offer different views, such as longitudinal, front, and back views. The dimensions are given in Table 1.

The results of the photon transport efficiency simulations of the second set of EGS configurations described in Figure 6 are shown in Table 5. Similar information is tabulated as for the first EGS set. Also, with this second set of EGS configurations, the systems with and without the hole, with the matted and unmatted scintillator exit side, were simulated to assess the effect of these differences. It is evident that the EGS configurations with the square plate scintillator are less efficient than those with the circular one. But greater differences in the LG efficiencies of the square and circular scintillators are only when connected to the strip light guides. By far the worst of all the configurations simulated in this paper is the strip configuration with the polished square plate scintillator that does not have a hole. This configuration has an extremely low mean efficiency of only 0.01%. It also has a low efficiency inhomogeneity over the electron excited scintillator surface.

The most efficient EGS configurations of this second set with the square scintillators are again those with the widening light guides. They achieve efficiencies of up to about 6.6% and are only negligibly less efficient than the similar configurations of the first set with the circular scintillators. Also, the efficiency homogeneities of these configurations of this set are only slightly different from the homogeneities of similar configurations of the previous set. It follows that, from an efficiency point of view, it is irrelevant whether the widening EGS configurations of the scintillation detectors in SEM with the square or circular scintillators will be selected. However, from a machining point of view, the circular plate scintillators are much more advantageous.

In any case, even the most efficient simple nonoptimized EGS configurations are extremely inefficient. However, there are locations on the excited scintillator surface in the simulated simple EGS configurations, from which signal photon collection has an efficiency of up to 21%. This means that the biggest problem is the loss in signal photon collection only from a part of the excited scintillator surface. This issue needs to be addressed when optimizing the EGS configurations.

4 | DISCUSSION

First, attention should be paid to the SCIUNI simulation model and to the material characterization results, which give important input parameters for the MC simulation application for photon transport efficiency in the scintillation electron detector for SEM. Only then the simulation results can be discussed.

Each model includes certain simplifications. The SCIUNI MC simulation model also contains certain approximations. The shapes and dimensions of both scintillators and light guides do not represent any simplification or difficulty. Their accuracy is quite suitable for the MC simulation. The integration of optical processes is more problematic. One of the simplifications is that the SCIUNI model does not work with the wavelengths of the entire CL emission band of the scintillator, but only with the wavelength of the emission band center of 559 nm, which was assigned to the optical quantities for the simulation, such as the absorption coefficient and refractive index. This fact has a more significant influence on the effect of the absorption coefficients (especially of that of the YAG:Ce scintillator), which show a greater dependence on the wavelength in the region of the YAG:Ce emission band than the refractive indices. However, the inaccuracy of the absorption coefficient effects is not significant. Some misgiving could only arise with absorption in the YAG:Ce scintillators

(0.743 cm^{-1}), but here the paths of the photons are only in the order of smaller units of mm. The longer photon paths can be in the PMMA light guides, but the absorption coefficient of PMMA is low in the whole area of the YAG:Ce emission band. Even at its shortwave edge it does not exceed 0.01 cm^{-1} . The photon paths in the optical cement are only about $20\text{ }\mu\text{m}$, so no inaccuracy in absorption losses in the optical cement can occur.

The inaccuracies regarding the narrowing of the emission band are negligible for the refractive indices because the values of the individual refractive indices are almost constant throughout the YAG:Ce emission band. This is important because even small differences in the refractive indices affect the optical reflectivity or optical transmissivity of different optical boundaries in the detection system, as shown in Figure 3. Unlike this Fresnel reflectivity, the internal mirror reflectivity at the Al interface shows no variability depending on the photon incidence angle, and its incorporation into the SCIUNI model is easier. Other approximations in the SCIUNI model have been published previously (Schauer, 2007; Schauer & Aufrata, 1992). In any case, all the simplifications in the SCIUNI application affect more the absolute magnitude of the transport efficiency and less the relative comparison of the efficiency of the different shapes and dimensions of the individual configurations. The lowest demands on the accuracy of the refractive index are for the NOA 61 optical cement. In principle, it is only necessary to fulfill the condition that the refractive index of the optical cement is lower than or equal to the refractive index of the scintillator and higher than or equal to the refractive index of the light guide.

It cannot be expected that the simulation of the signal photons transport from the luminescence centers of the simple scintillator - light guide configurations presented in this paper will provide a comprehensive answer on how to design and construct highly efficient scintillation detectors for SEM. Especially, if the simulation does not involve any optimization of the detection system and the results of the simulations are only the mean, minimum, and maximum photon transport efficiency from the randomly generated locations on the electron excited scintillator surface. However, the results of this paper can be used to find some rules that allow avoiding the design of completely inefficient configurations of these detectors.

The results of the efficiency simulation of the BGS configurations prove that the configuration with the disc scintillator with the matted exit side connected to the cylindrical light guide without optical cement is by far the most efficient and with the least dependence on the location of the luminescent centers. Such a configuration is the most efficient of all the simple BGS and EGS configurations presented in this paper. It is not important to use other than the circular plate (disc) scintillators in the rotationally symmetric BGS scintillation systems.

On the contrary, the BGS configuration with the same disc scintillator connected to the same cylindrical light guide with optical cement is very inefficient. The reason is that the completely cylindrical configurations with no diffuse surface cannot utilize photons whose angle of incidence on the internal scintillator or light guide walls is less than the critical angle, the values of which for the different boundaries are

evident from Figure 3. In other words, the completely cylindrical configurations with no diffuse surface suffer by the effect of the unchanging photon trajectory angle. For the BGS configurations with the conical or hemispherical scintillator this is not valid. That's why it is advantageous to use the optical cement to connect exit surfaces of the conical or hemispherical scintillators. The LG efficiency increase of the disc scintillator with the matted exit side connected to the cylindrical light guide without optical cement has been experimentally measured by many decades ago (Schauer & Aufrata, 1979). However, the measured increase in the LG efficiency is less distinctive compared to the simulation because ideal polished material is unlike the real free of diffuse surfaces. As is clear from the results of our previous paper (Schauer et al., 2021), using the BGS configuration with the conical scintillator cemented to the light guide is more advantageous only in the case of predominant signal electron collection at the axis of the detection system. In any case, designing the BGS configuration for SE detection is much simpler than designing the EGS one for BSE detection. In general, to ensure a satisfactory (about 20%) efficiency of signal photons transport from the luminescence centers in the BGS configurations, it is sufficient to apply a disk scintillator of the required size with the matted exit side connected to the cylindrical light guide without optical cement.

The design of EGS configurations for BSE detection is more complex. Even so, it is possible to determine certain rules for the design and construction of EGS configurations. From the results in Table 4 and Table 5, it is clear that the strip EGS configurations must be completely discarded. These poor configurations, which never achieve a mean photon transport efficiency of 0.7%, and which sometimes show efficiencies as low as only 0.01%, pay for their parallelism. This is because the parallelepiped configurations with no diffuse surface suffer by the effect of the unchanging photon trajectory angle (even more than the cylindrical configurations). All these extremely poor strip configurations also have the greatest efficiency inhomogeneity over the electron excited scintillator surface.

One way to break the regularity of the parallelepiped EGS configurations and thus change the disadvantageous angles of photon incidence on the internal light guide walls is to use the widening light guides. In other words, the widening systems are better because they can straighten the photons' trajectories towards the photocathode, but not from all locations of the scintillator surface, as was presented in our previous paper (Schauer et al., 2021). It is not important whether the light guide widening to the square profile or the circular one is used. The difference in efficiency between these two widening light guides is not greater than about 1%. However, the configuration with the widening to the circular profile is more advantageous because its machining is mostly rotationally symmetrical. Similarly, it is not important whether the circular plate scintillators or the square ones are used in the EGS configurations. The difference in efficiency between these two scintillator shapes is about 6% in favor of the circular scintillator. Again, the circular scintillator is more advantageous in terms of its production. Sometimes even a hole in the scintillator disrupts the unfavorable direction of the signal photons. Therefore, many simple EGS configurations with a hole can be more efficient

than those without a hole. In general, it may also help to matte the scintillator exit side, but the application of optical cement, which cannot be avoided, largely eliminates matting.

The effect of inclination of the EGS widening systems was not simulated to compare the simple configurations in this paper. However, based on our previous studies (Schauer, 2007; Schauer et al., 2021), it can be deduced that optimized inclinations will several times increase efficiency differences between the EGS strip and widening configurations in favor of the widening ones. A major and common problem of the simple nonoptimized EGS configurations is the poor homogeneity of photon transport efficiency over the electron excited scintillator surface. With these EGS systems, light collection from the scintillator locations adjacent to the light guide is much more efficient. Numerically expressed, signal photon collection from the scintillator locations close to the light guide achieves an efficiency of up to 21% compared to a mean efficiency of about 7% over the entire scintillator surface. This issue needs to be addressed when optimizing the EGS configurations.

However, it is not easy to obtain optimized EGS configurations without applying a COD. Based on COD performed in our previous papers (Schauer, 2007; Schauer et al., 2021), it can be concluded that it is possible to increase light collection from the scintillator locations remote from the light guide. But optimization of the individual simple geometric configurations was not the goal of this paper. Therefore, very time-consuming COD was not performed for these simple EGS configurations. The aim was to compare different detector shapes, not dimensions, and inclinations for individual shapes. Even so, it is clear from the mentioned previous studies that the angle of inclination and the origin of the light guide widening planes are important. The rule can be deduced that both widening planes must be shifted as close to the scintillator exit surface as possible. In our previous studies was also found that both widening planes must have the same slight inclination. However, a slight inclination of the planes is disadvantageous close to the scintillator. A gradual widening of the EGS configuration, shifting this widening as close to the scintillator as possible, optimizing its angle to the system axis, and integrating a conical LG ring close to the scintillator contributes to the arrangement of the photon trajectories longitudinally with the system axis. Such an arrangement helps increase the mean LG efficiency of the EGS configurations to as high as about 20% (Schauer et al., 2021).

It can be expected that optimizing the simple basic configurations presented in this paper would lead to increased efficiency. However, a lack of optimization simulation raises a question whether the relationship between the LG efficiencies of the individual shapes remains preserved after optimization. It cannot be answered with certainty without simulation. But according to optimization experience, it is very likely that more efficient design remains more efficient even after optimization (Schauer, 2007). It is also important to mention that optimization of only the size and slopes never resulted in a significant increase in the efficiency. The significant increase can be achieved only by using a more complex geometry, for example using a multiple-slope widening.

5 | CONCLUSION

The results of the photon transport efficiency simulations in the simple scintillator - light guide configurations presented in this paper show that the efficiency of light signal collection in such systems can be extremely low. The low transport efficiency of the signal photons affects the performance of the entire scintillation electron detector in SEM. However, most studies of SEM electron detector performance ignore this fact. Much more space is mostly devoted to the energy conversion in the scintillator than the utilization of the converted light signal (Everhart & Thornley, 2004; Frank, 2002; Healy & Mott, 2016; Nedela et al., 2018).

Although the SCIUNI application used to simulate photon transport efficiency is based on a model involving certain simplifications, mainly concerning the narrowing of the emission band, the simulation results presented in this paper allow a good comparison of the performance of the individual LG configurations. Although it was not expected that the simulation of only the simple LG configurations resulting in only the mean, minimum, and maximum efficiency, presented in this paper, will provide a comprehensive answer on how to design and construct highly efficient scintillation detectors for SEM, the results provide some rules to avoid the design of inefficient configurations. The basis of the usable results from this paper is also the quality CL and optical characterization of the used detector components, the results of which are presented here.

There is a big difference between the design requirements of the symmetric BGS configurations for secondary electron (SE) detection and the edge-guided signal (EGS) configurations for backscattered electron (BSE) detection, both in terms of design complexity and in terms of the photon collection efficiency. With some experience, it is even possible to estimate the shape of an efficient BGS configuration. Therefore, it is not surprising that the configuration with the disc scintillator with the matted exit side connected to the cylindrical light guide without optical cement is by far the most efficient and with the least dependence on the location of the luminescent centers.

The design of the EGS configurations is more complex. Almost every EGS configuration is less efficient than any BGS one. The use of completely inefficient EGS strip configurations must be avoided. These configurations are not only inefficient, but they also have the greatest efficiency inhomogeneity over the electron excited scintillator surface. The widening EGS systems are better because they can straighten the photons' trajectories towards the photocathode. It is not important whether the light guide widening to the square profile or the circular one is used. Similarly, it is not important whether the circular plate scintillators or the square ones are used in the EGS configurations. However, the circular profile is more advantageous because its machining is mostly rotationally symmetrical.

For a better conclusion about the EGS configurations, it would be interesting to complete simulations of the simple systems with simulations with different inclinations and positions of the widening planes. This has not yet been done in this paper. However, if we take into account the results from our previous papers (Schauer, 2007; Schauer et al., 2019; 2021), more rules for the widening of the most efficient

EGS configurations can be established. For example, the rules that both widening planes of such configurations must be shifted as close to the scintillator exit surface as possible and that both widening planes must have the same slight inclination. However, a slight inclination of the planes is disadvantageous close to the scintillator, so gradual widenings of the EGS configurations are the best solution.

In summary, the perfectly designed LG part of the scintillation detector with high photon transport efficiency is a significant benefit of the entire imaging system in SEM. Low-photon transport efficiency can significantly reduce detector performance. This is valid especially for the design of EGS configurations for BSE detection. When designing such systems, the strip configurations must be avoided. These strip configurations have an extremely low mean LG efficiency of only 0.01%. On the other hand, if a suitable COD application for optimization of the geometry and materials of EGS is used, we can get and utilize the EGS configuration reaching a mean LG efficiency as high as about 20%.

ACKNOWLEDGMENTS

The author thanks Jaroslav Sobota and Tomas Fort from the Institute of Scientific Instruments of the CAS, Brno, Czech Republic, for sputtering the conductive coatings. He also thanks the company Crytur, Turnov, Czech Republic, for the supply of the YAG:Ce single crystal scintillator. This research was supported by the Technology Agency of the Czech Republic (project TN01000008). The research infrastructure was funded by the Czech Academy of Sciences (project RVO:68081731).

DATA AVAILABILITY STATEMENT

Data are available from the corresponding author upon reasonable request.

ORCID

Petr Schauer  <https://orcid.org/0000-0002-7930-0983>

REFERENCES

- Badiei, S., Raisali, G., Kardan, M., Moslehi, A., & Rezaeian, P. (2019). Development and validation of a Geant4 application to calculate the response matrix of a set of superheated drop detectors under various external pressures. *Nuclear Instruments & Methods in Physics Research Section a-Accelerators Spectrometers Detectors and Associated Equipment*, 939, 55–60.
- Bauer, F., Corbeil, J., Schmand, M., & Henseler, D. (2009). Measurements and ray-tracing simulations of light spread in LSO crystals. *IEEE Transactions on Nuclear Science*, 56(5), 2566–2573.
- Bok, J., & Schauer, P. (2014a). Apparatus for temperature-dependent cathodoluminescence characterization of materials. *Measurement Science and Technology*, 25(7), 75601.
- Bok, J., & Schauer, P. (2014b). Performance of SEM scintillation detector evaluated by modulation transfer function and detective quantum efficiency function. *Scanning*, 36(4), 384–393.
- Born, M., & Wolf, E. (1999). *Principles of optics: Electromagnetic theory of propagation, interference and diffraction of light*. Cambridge University Press.
- Carrier, C., & Lecomte, R. (1990a). Effect of geometrical modifications and crystal defects on light collection in ideal rectangular Parallelepipedic Bgo scintillators. *Nuclear Instruments & Methods in Physics Research Section a-Accelerators Spectrometers Detectors and Associated Equipment*, 294(1–2), 355–364.
- Carrier, C., & Lecomte, R. (1990b). Theoretical modeling of light transport in rectangular Parallelepipedic scintillators. *Nuclear Instruments & Methods in Physics Research Section a-Accelerators Spectrometers Detectors and Associated Equipment*, 292(3), 685–692.
- Comins, N. R., & Thirlwall, J. T. (1981). Quantitative studies and theoretical-analysis of the performance of the scintillation electron-detector. *Journal of Microscopy*, 124(Nov), 119–133.
- Danilatos, G. D. (2012). Backscattered electron detection in environmental SEM. *Journal of Microscopy*, 245(2), 171–185.
- Everhart, T. E., & Thornley, R. F. M. (2004). Wide-band detector for microampere low-energy electron currents. *Advances in Imaging and Electron Physics*, 133, 147–152.
- Filippov, M. N., Rau, E. I., Sennov, R. A., Boyde, A., & Howell, P. G. T. H. (2001). Light collection efficiency and light transport in backscattered electron scintillator detectors in scanning electron microscopy. *Scanning*, 23(5), 305–312.
- Frank, L. (2002). Advances in scanning electron microscopy. *Advances in Imaging and Electron Physics*, 123, 327–373.
- Goodman, J. W. (2005). *Introduction to Fourier optics*. Roberts and Company Publishers.
- Healy, O. E., & Mott, R. B. (2016). Real-world electron detector performance in scanning electron microscopes. *Microscopy and Microanalysis*, 22(S3), 596–597.
- Joy, D. C., Joy, C. S., & Bunn, R. D. (1996). Measuring the performance of scanning electron microscope detectors. *Scanning*, 18(8), 533–538.
- Knittel, Z. (1976). *Optics of thin films.(an optical multilayer theory)*. John Wiley & Sons.
- Knyazev, A., Park, J., Golubev, P., Cederkäll, J., Alvarez-Pol, H., Benlliure, J., Cabanelas, P., Casarejos, E., Causeret, L., & Cortina-Gil, D. (2021). Simulations of light collection in long tapered Csl (TI) scintillators using real crystal surface data and comparisons to measurement. *Nuclear Instruments and Methods in Physics Research Section A: Accelerators, Spectrometers, Detectors and Associated Equipment*, 1003, 165302.
- Kuwano, Y., Saito, S., & Hase, U. (1988). Crystal-growth and optical-properties of Nd-Ggag. *Journal of Crystal Growth*, 92(1–2), 17–22.
- Lerche, C. W., Ros, A., Herrero, V., Esteve, R., Monzo, J. M., Sebastia, A., Sanchez, F., Munar, A., & Benloch, J. M. (2008). Dependency of energy-, position- and depth of interaction resolution on scintillation crystal coating and geometry. *IEEE Transactions on Nuclear Science*, 55(3), 1344–1351.
- Lorincz, E., Erdei, G., Peczei, I., Steinbach, C., Ujhelyi, F., & Bukki, T. (2010). Modeling and optimization of scintillator arrays for PET detectors. *IEEE Transactions on Nuclear Science*, 57(1), 48–54.
- Nedela, V., Tihlarikova, E., Runstuk, J., & Hudec, J. (2018). High-efficiency detector of secondary and backscattered electrons for low-dose imaging in the ESEM. *Ultramicroscopy*, 184, 1–11.
- Norland (2021). Norland optical adhesive. Technical information on NOA 61, Norland Products. <https://www.norlandprod.com/adhesives/NOA%2061.html>.
- Oatley, C. W. (1985). The detective quantum efficiency of the scintillator photomultiplier in the scanning electron-microscope. *Journal of Microscopy-Oxford*, 139, 153–166.
- Ohlidal, I., & Navrátil, K. (1984). Spectroscopic methods for optical analysis of thin films. *Folia facultatis scientiarum naturalium Universitatis Purkynianae Brunensis. Mathematica - Physica*, 25(37), 5–83.
- Reimer, L. (2013a). Backscattered electron detectors. In *Scanning electron microscopy: Physics of image formation and microanalysis*. Springer-Verlag.
- Reimer, L. (2013b). Detector noise. In *Scanning electron microscopy: Physics of image formation and microanalysis*. Springer-Verlag.
- Reimer, L. (2013c). *Scanning electron microscopy: Physics of image formation and microanalysis*. Springer-Verlag.

- Reimer, L. (2013d). Secondary and backscattered electron detectors. In *Scanning electron microscopy: Physics of image formation and microanalysis*. Springer-Verlag.
- Robinson, V. N. E. (1980). Imaging with backscattered electrons in a scanning electron-microscope. *Scanning*, 3(1), 15–26.
- Saiga, R., Takeuchi, A., Uesugi, K., Terada, Y., Suzuki, Y., & Mizutani, R. (2018). Method for estimating modulation transfer function from sample images. *Micron*, 105, 64–69.
- Salomoni, M., Pots, R., Auffray, E., & Lecoq, P. (2018). Enhancing light extraction of inorganic scintillators using photonic crystals. *Crystals*, 8(2), 78.
- Schauer, P. (2007). Extended algorithm for simulation of light transport in single crystal scintillation detectors for S(T)EM. *Scanning*, 29(6), 249–253.
- Schauer, P., & Aufrata, R. (1979). Electro-optical properties of a scintillation detector in Sem. *Journal De Microscopie Et De Spectroscopie Electroniques*, 4(6), 633–650.
- Schauer, P., & Aufrata, R. (1992). Light transport in single-crystal scintillation detectors in SEM. *Scanning*, 14(6), 325–333.
- Schauer, P., & Aufrata, R. (2000). Performance of detector elements for electron microscopes. *Fine Mechanics and Optics*, 45(10), 268–270.
- Schauer, P., Lalinsky, O., & Kucera, M. (2019). Prospective scintillation electron detectors for S(T)EM based on garnet film scintillators. *Microscopy Research and Technique*, 82(3), 272–282.
- Schauer, P., Lalinsky, O., & Kucera, M. (2021). Overview of S(T)EM electron detectors with garnet scintillators: Some potentials and limits. *Microscopy Research and Technique*, 84(4), 753–770.
- van der Laan, D. J., Schaart, D. R., Maas, M. C., Beekman, F. J., Bruyndonckx, P., & van Eijk, C. W. E. (2010). Optical simulation of monolithic scintillator detectors using GATE/GEANT4. *Physics in Medicine and Biology*, 55(6), 1659–1675.
- Williams, C. S., & Becklund, O. A. (2002). *Introduction to the optical transfer function*. SPIE Press.
- Williams, T. (1998). *The optical transfer function of imaging systems*. Taylor & Francis.
- Xiaoguang, Y. (1984). A study of light collection efficiency in scintillation detectors. *Nuclear Instruments and Methods in Physics Research Section A: Accelerators, Spectrometers, Detectors and Associated Equipment*, 228(1), 101–104.
- Zhou, W., Apkarian, R., Wang, Z. L., & Joy, D. (2006). Fundamentals of scanning electron microscopy (SEM). In *Scanning microscopy for nanotechnology* (pp. 1–40). Springer.

How to cite this article: Schauer, P. (2022). Comparison of photon transport efficiency in simple scintillation electron detector configurations for scanning electron microscope. *Microscopy Research and Technique*, 85(5), 1870–1883. <https://doi.org/10.1002/jemt.24048>